Chemical Geology 405 (2015) 48–62

Contents lists available at ScienceDirect

Chemical Geology

journal homepage: www.elsevier.com/locate/chemgeo

Redox architecture of an Ediacaran ocean margin: Integrated chemostratigraphic ($\delta^{13}C$–$\delta^{34}S$–$^{87}Sr/^{86}Sr$–Ce/Ce*) correlation of the Doushantuo Formation, South China

Huan Cui [a,*], Alan J. Kaufman [a,b], Shuhai Xiao [c], Maoyan Zhu [d], Chuanming Zhou [d], Xiao-Ming Liu [e]

[a] Department of Geology, University of Maryland, College Park, MD 20742, USA
[b] Earth System Science Interdisciplinary Center, University of Maryland, College Park, MD 20742, USA
[c] Department of Geosciences, Virginia Tech, Blacksburg, VA 24061, USA
[d] State Key Laboratory of Palaeobiology and Stratigraphy, Nanjing Institute of Geology and Palaeontology, Chinese Academy of Science, Nanjing 210008, China
[e] Geophysical Laboratory, Carnegie Institution of Washington, Washington, D.C. 20015, USA

ARTICLE INFO

Article history:
Received 4 September 2014
Received in revised form 9 April 2015
Accepted 11 April 2015
Available online 19 April 2015

Editor: Michael E. Böttcher

Keywords:
Ediacaran
Doushantuo Formation
Redox model
Euxinia
Shuram Excursion
Chemostratigraphy

ABSTRACT

Early diagenetic silicification and phosphatization of the Ediacaran Doushantuo Formation (ca. 635 to 551 Ma) in South China offer extraordinary taphonomic windows into the early evolution of multicellular eukaryotes, including various algal groups and potentially animals. In order to understand how the ecological and taphonomic distribution of these Ediacaran eukaryotes was controlled by oceanic redox conditions, it is critical to reconstruct the redox architecture of the sedimentary basin. Recently two alternative redox models have been proposed to account for the geochemical and sedimentary features of the Doushantuo Formation. One argues that the unit was deposited on a continental margin where a metastable sulfidic wedge was dynamically maintained by a sulfate concentration gradient between shelf and basinal environments. The other contends that the sulfidic water mass was largely restricted to the intra-shelf basin behind a rimmed margin. These two models make different predictions about the stratigraphic completeness and correlation of the Doushantuo Formation. To test these predictions, we generated high-resolution time-series trends of multiple isotopic and elemental tracers, including $\delta^{34}S$, $^{87}Sr/^{86}Sr$ and Ce/Ce*, to facilitate an integrated chemostratigraphic correlation between inner shelf (Xiaofenghe), intra shelf (Jiulongwan), and outer shelf (Yangjiaping and Zhongling) sections. Our correlations suggest that both the inner and outer shelf sections are stratigraphically incomplete relative to the intra shelf section. The euxinic wedge model should be reconsidered insofar as it is based on a miscorrelation between sections. Viewed from our revised chemostratigraphic framework, euxinic conditions on the platform appear to have been largely restricted to the intra shelf basin. Carbonates in the upper Doushantuo Formation at Jiulongwan and their stratigraphic equivalents are characterized by a profound negative carbon isotope anomaly (i.e., the Shuram Excursion) coincident with a drop in pyrite sulfur isotope values and a significant rise in $^{87}Sr/^{86}Sr$ from 0.7080 to 0.7090. The integrated stratigraphic data from South China suggest that the onset of the Shuram Excursion is associated with enhanced oxidative continental weathering that delivered radiogenic strontium, as well as sulfate, to the Ediacaran basin.

1. Introduction

The unrestricted Modern ocean is pervasively oxygenated from the surface to the abyssal deep (with oxygen content ranging from 3.5 to 7 mL/L depending on the salinity and temperature of various ocean masses) with the exception of oxygen minimum zones where the remineralization of particulate organic matter by aerobic bacteria draws the breathing gas to its lowest concentration (ca. 0.2 mL/L) (Deutsch et al., 2011). Nitrate can also become limiting in these zones as denitrifying bacteria use the oxidant for respiration. Animals living in oxygen minimum zones must either have a reduced metabolic rate or be very efficient at extracting O_2 from seawater. Some of these animals have evolved to have large gill surface areas, resulting in short diffusion distances from the water to the blood. Given that even the simplest animals require a few percent of present atmospheric levels (Mills et al., 2014) and more complex organisms need much more to engage in more active life styles, it is important to understand the redox state of the water column and how oxygen contents in shallow marine ecosystems might be modified by future global warming (Mora et al., 2013).

Determining the redox architecture of ancient ocean margins is particularly important in the Ediacaran Period (635 to 541 Ma) when the first large complex life forms (including animals) evolved (Xiao and

* Corresponding author.
E-mail address: hcui@umd.edu (H. Cui).

http://dx.doi.org/10.1016/j.chemgeo.2015.04.009
0009-2541/

Laflamme, 2009), assuming the Ediacara biota required O_2 for their metabolic activities and acquired the gas through diffusion (Laflamme et al., 2009). Most, if not all, fossils of the Ediacara biota appear in the sedimentary record following a profound negative carbon cycle anomaly known as the Shuram Excursion (Grotzinger et al., 2011; Macdonald et al., 2013) named after strata in Oman where the event was first described (Burns and Matter, 1993). During this event the carbon isotopic compositions of bedded carbonates, including some oolitic and stromatolitic facies (cf. Melezhik et al., 2009; Lu et al., 2013), fell to a nadir of less than −10‰ and stabilized for millions of years before returning to pre-event conditions. This profound negative carbon cycle anomaly has been interpreted in various ways, including 1) modification of global seawater compositions through oxidation of dissolved organic compounds in the oceans (Rothman et al., 2003), fossil organic carbon exposed on land (Kaufman et al., 2007), or methane in clathrates (Bjerrum and Canfield, 2011), 2) mixing of normal seawater precipitates with authigenic carbonates of anomalous isotopic composition formed through anaerobic metabolic activities (Schrag et al., 2013), or 3) alteration of carbonate sediments through interaction with diagenetic fluids of terrestrial origin (Knauth and Kennedy, 2009; Derry, 2010).

The Shuram Excursion is well developed in Ediacaran successions throughout South China (Jiang et al., 2007, 2011; Zhu et al., 2007; McFadden et al., 2008; Wang et al., 2012; Lu et al., 2013; Zhu et al., 2013; Tahata et al., 2013), including the well-studied intra-shelf section near Jiulongwan (Fig. 1A, B) where the onset of the carbon isotope event occurs in dolostone and limestone facies immediately above a thick cherty horizon (McFadden et al., 2008). Notably, in both the proximal inner shelf section at Xiaofenghe, as well as the distal outer shelf sections at Zhongling and Yangjiaping, the Shuram carbon isotope anomaly is missing altogether, or is very poorly expressed (Zhu et al., 2007; Li et al., 2010; Kunimitsu et al., 2011; Xiao et al., 2012; Liu et al., 2013; Zhu et al., 2013). Based on iron-speciation analyses and a clear sulfur isotope contrast between sections in the uppermost Doushantuo Formation at Jiulongwan and Zhongling (believed at the time to represent deep water deposition on the continental slope), Li et al. (2010) proposed that a metastable euxinic wedge was maintained dynamically across the ramp by a gradient of sulfate concentration between shallow and deep settings (Fig. 1C). Such redox modeling is based on the assumption that sections of the Doushantuo Formation in inner shelf Jiulongwan and outer shelf Zhongling section are continuous and well correlated (see Fig. S7 of Li et al., 2010). Sedimentary facies analyses, however, suggest that the sections at Zhongling and nearby Yangjiaping accumulated in shallow waters along an elevated margin rim, suggesting that euxinic conditions on the platform may have been restricted to an intra shelf setting (Zhu et al., 2007; Jiang et al., 2011; Zhu et al., 2013). Similar conditions may have also characterized deep-water slope settings distal from the rimmed shelf based on the preponderance of framboidal relative to euhedral pyrite preserved in the sediments and abundances of redox-sensitive trace elements (Fig. 1D; Sahoo et al., 2012; Wang et al., 2012). These observations suggest that euxinia may have been patchy across Doushantuo margin environments, and that the wedge model needs to be reconsidered in light of improved stratigraphic correlation and integrated geochemical data.

To search for the Shuram Excursion in the outer shelf environments preserved at Zhonging and Yangjiaping (~90 km to the southwest of Jiulongwan) where phosphorite is abundant in the upper reaches of the Doushantuo Formation, and to test the hypothesis that the shoal complex in this setting is stratigraphically incomplete, we applied time-series $\delta^{13}C$, $\delta^{34}S$, and $^{87}Sr/^{86}Sr$ isotope data from four sections (with Ce/Ce* from two of these) that span across the platform margin (Fig. 1E). The integrated results provide a systematic framework of chemostratigraphic correlations that allow us to test the two competing redox reconstructions for the Ediacaran basin. In addition, the time-series trends provide environmental context for the Laggerstätten of

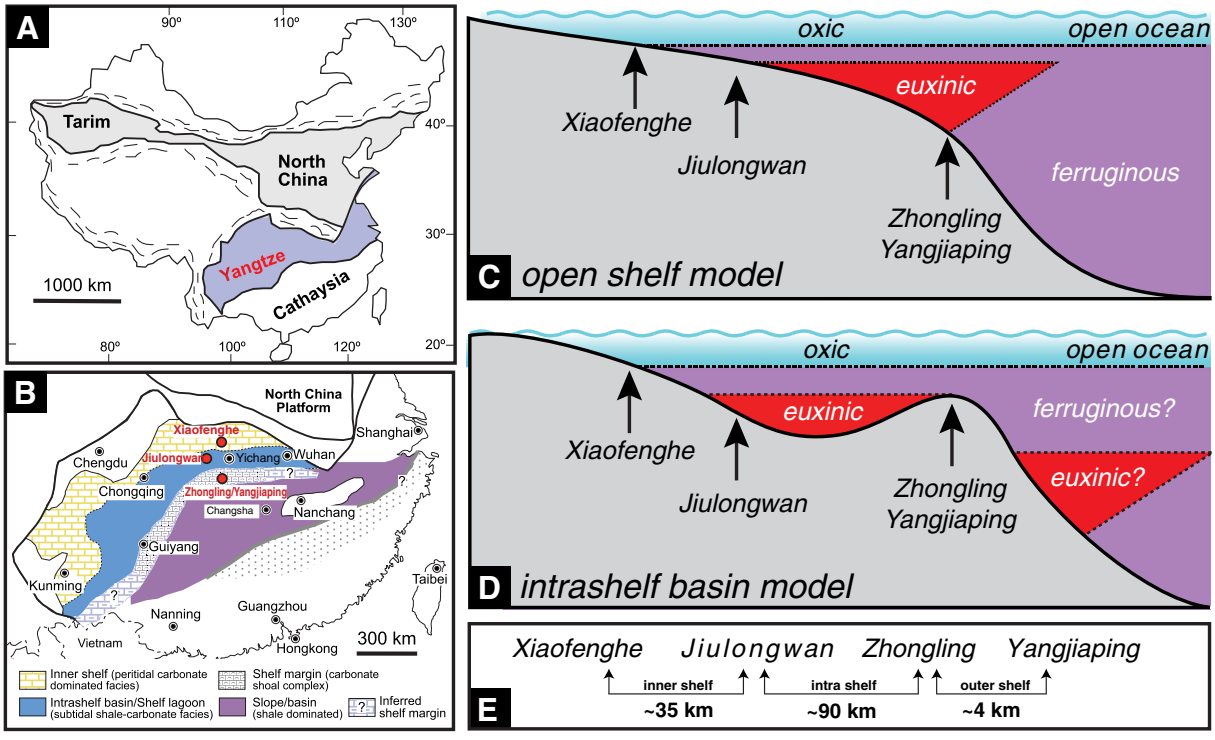

Fig. 1. (A) Geological map of China, with the Yangtze Craton highlighted in color. (B) Reconstructed Ediacaran depositional environments on the Yangtze Craton (Jiang et al., 2011). Red dots mark the location of the four sections discussed in this paper. (C) Open shelf model with a metastable sulfidic wedge maintained dynamically by overall low oceanic sulfate concentrations and a gradient of sulfate concentration between shallow and deep environments (Li et al., 2010). (D) Intra-shelf basin model with euxinic water mass largely restricted in lagoonal and deep basin settings (Jiang et al., 2011; Wang et al., 2012; Sahoo et al., 2012). (E) Distance between each correlated sections.

unicellular and multicellular eukaryotes preserved in the Doushantuo Formation, and also allow us to evaluate the role of continental weathering at a time of rising atmospheric oxygen as a critical driver of the Shuram Excursion.

2. Geologic setting

Ediacaran successions in South China that blanket the Yangtze block include the richly fossiliferous Doushantuo and Dengying formations. Abundant three-dimensionally preserved eukaryotes, including multicellular algae, sponge, putative animal embryos, and acritarchs, have been discovered from phosphorites and chert nodules of the Doushantuo Formation (Xiao et al., 1998, 2014; Liu et al., 2014; Muscente et al., 2015; Yin et al., 2015), while Dengying strata contain macroscopic Ediacara fossils and trace fossils (Chen et al., 2013, 2014; Meyer et al., 2014). The basal Doushantuo Formation is underlain by the Nantuo diamictite and begins with a ca. 635 Ma cap carbonate (Condon et al., 2005). In the Yangtze Gorges area, this formation is informally divided into four distinct members (McFadden et al., 2008) and is typically capped by black shale below massive dolostone of the Dengying Formation (Jiang et al., 2011). The boundary between the two formations is constrained in age to be <551 Ma (Condon et al., 2005), suggesting that the Doushantuo carbonate platform accumulated over a period of 84 Ma or more. Hence, the Doushantuo Formation is remarkably thin for the geological time it occupies. The mixed shale and carbonate in the inner shelf Jiulongwan section, which is well exposed along a road cut during the construction of the Yangtze Gorges Dam, has a thickness of only ~160 m. In contrast, the carbonate-rich outer shelf section at Zhongling and Yangjiaping have thicknesses of 260 and 180 m, respectively (Zhu et al., 2007; Jiang et al., 2011; Muscente et al., 2015). Continental slope and basinal environments of the Doushantuo Formation further to the southeast are significantly thinner and are dominated by fine-grained siliciclastics with only thin carbonate turbidite interbeds (Jiang et al., 2007; Zhu et al., 2007).

The Doushantuo Formation formed in two stages, with an open ramp shelf environment building up to a rimmed shelf protecting an intra-shelf lagoon (Jiang et al., 2011). Paleogeographic reconstructions of strata on the Yangtze Platform indicate an increase in the water depth from proximal intertidal environments in the northwest to distal deep basinal settings in the southeast. Three platform facies belts are apparent, including proximal inner shelf peritidal carbonates, an intra-shelf lagoon containing mixed carbonate and shale, and an outer shelf shoal complex (Fig. 1B). The Doushantuo section at Zhongling previously studied by Li et al. (2010) is representative of the shoal complex facies, as is the Yangjiaping section some four kilometers distant that was sampled in this study. At Zhongling and Yangjiaping, the Doushantuo Formation is mainly composed of interbeded shale and carbonate, with an increasing preponderance of intraclastic and oolitic facies up-section, indicating shallower and higher-energy depositional environments. The Doushantuo in the shoal complex is terminated by several phosphorite horizons that occur just below the overlying Dengying Formation (Fig. 2; Jiang et al., 2007; Jiang et al., 2011; Kunimitsu et al., 2011), which is characterized by massive dolostone deposited in peritidal environments.

3. Methods

3.1. Field sampling

In this study, the uppermost 100 m of the Doushantuo Formation at the Yangjiaping section and the entire Doushantuo Formation at the Zhongling section near the town of Hupingshan were sampled at a high resolution for petrographic observation and time-series elemental and isotope analysis. At the Yangjiaping section, the lower part of the section is poorly exposed beneath thick vegetation and was not sampled. The upper part of the Doushantuo is characterized by organic-rich oolitic limestone (Fig. 2I), with a thin interval containing shale and interbedded phosphorite breccia (Fig. 2K), which is immediately overlain by cherty dolostone of the Dengying Formation (Zhu et al., 2007). The Zhongling section (Fig. 2M, N, O) is lithostratigraphically similar, with oolitic (Fig. 2G, H) and intraclastic carbonates (Fig. 2D, E, F) near the top of the Doushantuo Formation, which are overlain by a prominent phosphorite horizon (Fig. 2D). All samples collected from these two sections were analyzed and archived in the Geochemical Laboratories at the Department of Geology, University of Maryland.

3.2. Elemental analyses

Approximately 5–7 mg of micro-drilled sample powders were weighted and dissolved in 2 mL distilled 0.4 M HNO_3. The resulting solutions were centrifuged and 1 mL of the supernatants were pipetted and diluted with distilled 3 mL 0.4 M HNO_3 for elemental analysis. Major, trace, and REE concentrations were determined with a Thermo Scientific® iCAP-Q ICP-MS (Inductively Coupled Plasma — Mass Spectrometry) at the Carnegie Institution for Science. Calibration curves were created using multi-elemental standards made from pure element solutions (Alfa Aesar®). Both standard and sample solutions were doped with 4 ppb In to correct for instrumental drift. Precision of the analyses determined by repeated analyses of a house standard carbonate were better than 5% (2σ) for major elements with high concentrations and better than 10% (2σ) for the REEs.

3.3. Carbonate carbon and oxygen isotope analyses

Carbonate carbon and oxygen isotopes were measured by continuous flow isotope ratio mass spectrometry in the University of Maryland Paleoclimate CoLaboratory using a refined method for the analysis and correction of carbon ($\delta^{13}C$) and oxygen ($\delta^{18}O$) isotopic compositions of 100 μg carbonate samples (Fig. S1; Spötl, 2011). Up to 180 samples loaded into 3.7 mL Labco Exetainer vials and sealed with Labco septa were flushed with 99.999% Helium and manually acidified at 60 °C. The carbon dioxide analyte gas was isolated via gas chromatography, and water was removed using a Nafion trap prior to admission into an Elementar Isoprime stable isotope mass spectrometer fitted with a continuous flow interface. Data were corrected via automated Matlab scripting on the Vienna PeeDee Belemnite and LSVEC Lithium Carbonate (VPDB-LSVEC) scale (Coplen et al., 2006) using periodic in-run measurement of international reference carbonate materials and/or in-house standard carbonates, from which empirical corrections for signal amplitude, sequential drift, and one or two-point mean corrections were applied. Precision for both isotopes is routinely better than 0.1‰. Including acidification, flush fill, reaction and analysis, true throughput exclusive of correcting standards is 2–3 samples/h, or up to 144 samples over a 40-hour analytical session.

3.4. Organic matter carbon and pyrite sulfur isotope analyses

The organic carbon and pyrite sulfur isotope compositions were measured by combustion to CO_2 or SO_2 with a Eurovector elemental analyzer in-line with a second Elementar Isoprime isotope ratio mass spectrometer (Fig. S1). Approximately 10 g of sample trimmed with a rock saw to remove weathered surfaces and secondary veins was crushed to 200 mesh and finer, and then repeatedly acidified with 3 M HCl and washed with ultra-pure Milli-Q water until the solution reached neutral pH. Decalcified residues were dried overnight and quantified to determine carbonate percentages, and then accurately weighed and folded into small tin cups.

For pyrite sulfur measurements, V_2O_5 was mixed with the decalcified residues (assuming pyrite S ≫ organic S) to enhance combustion to SO_2. The tin cups were sequentially dropped with a pulsed O_2 purge of 12 mL into a catalytic combustion furnace operating at 1030 °C. The frosted quartz reaction tube was packed with high purity reduced copper wire for quantitative oxidation and O_2 resorption. Water was removed from

the combustion products with a 10-cm $Mg(ClO_4)_2$ column, and the SO_2 was separated from other gases with a 0.8-m PTFE GC column packed with Porapak 50–80 mesh heated to 115 °C. The effluent from the elemental analysis (EA) was introduced in a flow of He (80–120 mL/min) to the IRMS through a SGE splitter valve that controls the variable open split. Timed pulses of SO_2 reference gas (Air Products 99.9% purity, ~3 nA) were introduced at the beginning of the run using an injector connected to the IRMS with a fixed open ratio split. The isotope ratios of reference and sample peaks were determined by monitoring ion beam intensities relative to background values. The cycle time for these analyses was 210 s with reference gas injection as a 30-second pulse beginning at 20 s. Sample SO_2 pulses begin at 110 s and return to baseline values between 150 and 180 s, depending on sample size and column conditions. Sulfur isotope ratios were determined by comparing integrated peak areas of m/z 66 and 64 for the reference and sample SO_2 pulses, relative to the baseline that is approximately 1×10^{-11}A. The background height was established from the left limit of the sample SO_2 peak. Isotopic results are expressed in the delta notation as per mil (‰) deviations from the Vienna Canyon Diablo Troilite (V-CDT) standard. Two NBS 127 barite standards and two IAEA NZ1 silver sulfide standards were measured between each set of 10 samples and uncertainties for each analytical session based on these standard analyses were determined to be better than 0.3‰.

Measurements for organic carbon abundance and isotope composition with the elemental analyzer and isotope ratio mass spectrometer were similar to those of sulfur, except that the reaction column was packed with chromium oxide and silvered cobaltous/cobaltic oxide and heated to 1040 °C and the analyte also flows through a second column at 1040 °C packed with high purity reduced copper wire for quantitative reduction of NO_2 and N_2O and O_2 resorption. The CO_2 was separated from other gases with a 3-m stainless steel GC column packed with Porapak-Q heated to 60 °C. Timed pulses of CO_2 reference gas (Airgas 99.999% purity, ~6 nA) were introduced at the beginning of the run using an injector connected to the IRMS with a fixed open ratio split. The isotope ratios of reference and sample peaks were determined by monitoring ion beam intensities relative to background values. The cycle time for these analyses was 430 s with reference gas injection as two a 30-s pulse beginning at 15 and 60 s. Sample CO_2 peaks begin at 200 s and return to baseline around 240 s. Carbon isotope ratios were determined by comparing integrated peak areas of m/z 45 and 44 for the reference and sample CO_2 pulses, relative to the baseline that is approximately 2×10^{-11} A. The background height was established from the left limit of the sample CO_2 peak. Isotopic results are expressed in the delta notation as per mil (‰) deviations from the Vienna Pee Dee Belemnite (V-PDB) standard. Two urea standards were measured between each set of 10 samples and uncertainties for each analytical session based on these standard analyses were determined to be better than 0.1‰.

3.5. Strontium isotope analyses

For analysis of strontium isotopic ($^{87}Sr/^{86}Sr$) composition, only limestone/calcite samples were selected for extraction and measurement. Micro-drilled powders (ca. 5–10 mg) were leached three times in 0.2 M ammonium acetate (pH ~ 8.2) to remove exchangeable Sr from non-carbonate minerals, and then rinsed three times with Milli-Q water. The leached powder was centrifuged, decanted, and acidified with doubly distilled 0.5 M acetic acid overnight to remove strontium from the carbonate crystal structure. The supernatant was centrifuged to remove insoluble residues and then decanted, dried, and subsequently dissolved in 200 μL of 3 M HNO_3. Strontium separation by cation exchange was carried out using a small polyethylene column containing ~1 cm of Eichrom®Sr specific resin. The column was rinsed with 400 μL of 3 M HNO_3 before the dissolved sample was loaded onto the column. After loading, the sample was sequentially eluted with 200 μL of 3 M HNO_3, 600 μL of 7 M HNO_3, and 100 μL of 3 M HNO_3 to remove the Ca, Rb and REE fractions; the Sr fraction adsorbs strongly to the resin in an acidic environment. The Sr fraction was removed by elution with ~800 μL of 0.05 M HNO_3 and the resultant eluate collected and dried. Approximately 200–300 ng of the dried sample was transferred onto a degassed and pre-baked (~4.2 A under high vacuum) high purity Re filament with 0.7 μL of Ta_2O_5 activator. The prepared filaments were measured using the VG Sector 54 thermal ionization mass spectrometer in the TIMS facility of the University of Maryland Geochemistry Laboratories (Fig. S1). Filaments were transferred to a sample carousel, heated under vacuum (~10^{-7} to 10^{-8} atm) to a temperature between 1450 and 1650 °C, and analyzed when a stable signal (>1.0 V) was detected on the mass 88 ion beam. Approximately 100 $^{87}Sr/^{86}Sr$ ratios were collected for each sample. Final data have been corrected for fractionation using the standard value $^{86}Sr/^{88}Sr = 0.1194$. The fraction of ^{87}Sr resulting from in situ decay from ^{87}Rb was removed by measurement of rubidium abundance at mass 85. Repeated analysis of the NBS SRM987 standard yields an average value of $^{87}Sr/^{86}Sr = 0.710245 \pm 0.000011$ (2σ) during the analytical window.

4. Results

In this study, we systematically measured carbonate (wt.%, major and trace element concentrations, $\delta^{13}C_{carb}$, $\delta^{18}O$, and $^{87}Sr/^{86}Sr$), organic matter (wt.% and $\delta^{13}C_{org}$), and pyrite (wt.% and $\delta^{34}S_{pyrite}$) compositions in samples from the upper part of Doushantuo Formation at the Yangjiaping section (Fig. 3; supplemental data Table S1). Carbonate abundance of most bulk sample powders were >80% with the exception of a few samples near the bottom and top of the succession. Based on element ratios all samples have very low Mn/Sr ratio (ranging from 0.01 to 0.18), Fe/Sr (ranging from 0.18 to 17.17), and Rb/Sr (ranging from 0.0002 to 0.0154). Rare earth element concentrations were low as expected for carbonates, and were normalized to PAAS (Post Archean Australian Shale) in order to calculate the magnitude of Ce anomalies $Ce/Ce^* = Ce_{PAAS} / ([Pr]^2_{PAAS} / [Nd]_{PAAS})$ as presented by Ling et al. (2013). The Ce/Ce* ratios of the Yangjiaping samples ranged from 0.3 to 0.9 with significant oscillations through the succession, including a noted increase in values from samples in the uppermost 30 m. Carbon isotope compositions of micro-drilled powders are relatively invariant with $\delta^{13}C$ values of +5‰ in most of the Yangjiaping section except in the three samples from the uppermost 10 m; these reveal a decreasing trend from ca. +5‰ to a nadir value of −6.8‰. Similarly, the $\delta^{18}O$ values of the limestone samples are relatively invariant. Organic carbon isotope data ($\delta^{13}C_{org}$) range between −20 and −30‰ with a slight deceasing trend at the top of the section. Based on the measured carbonate carbon and organic carbon isotope values in individual samples, we calculated the magnitude of carbon isotope fractionation ($\Delta\delta^{13}C$). The $\Delta\delta^{13}C$ values average around 30‰ through most of the measured section, with the exception of a slightly decreasing trend to ~22‰ in the upper 30 m. Pyrite sulfur isotope data show highly positive values (average ca. +20‰) throughout the section. Strontium isotope ($^{87}Sr/^{86}Sr$) data reveal steady values of ~0.7080 throughout most of the succession, except in the upper 20 m where $^{87}Sr/^{86}Sr$ ratios rise up to a maximum of 0.7085 as recorded in phosphatic limestones.

The Zhongling samples were also analyzed for organic carbon, pyrite sulfur and strontium isotope compositions, in order to test regional variations and to facilitate chemostratigraphic correlation with the Yangjiaping section. The data are presented in supplemental data Table S2. Organic carbon isotope data in Zhongling show consistent values of ca. −25‰ in most of the section, except some more negative values (ca. −30‰) in the basal cap carbonate. Pyrite sulfur isotope data range between +20‰ to +40‰, with a slight decrease to ca. +20‰ near the top. Strontium isotope data shows consistent value of ca. 0.7080 in most of the section, with a sudden rise to 0.7083 in the upper 20 m.

5. Discussion

5.1. Diagenesis

To evaluate the degree of preservation of the Yangjiaping and Zhongling samples, we investigated the petrography, elemental and isotope geochemistry of the samples, which were collected in a sedimentological and stratigraphic context. These measurements and observations allow for field and laboratory tests of the fidelity of the time-series isotope records. First, the outcrop samples used in this study were primarily composed of fine-grained limestone, although in the upper 20 m of the section at Yangjiaping dolostone and phosphatic limestone were also sampled. Various phases were micro-sampled from polished billets to avoid weathered surfaces,

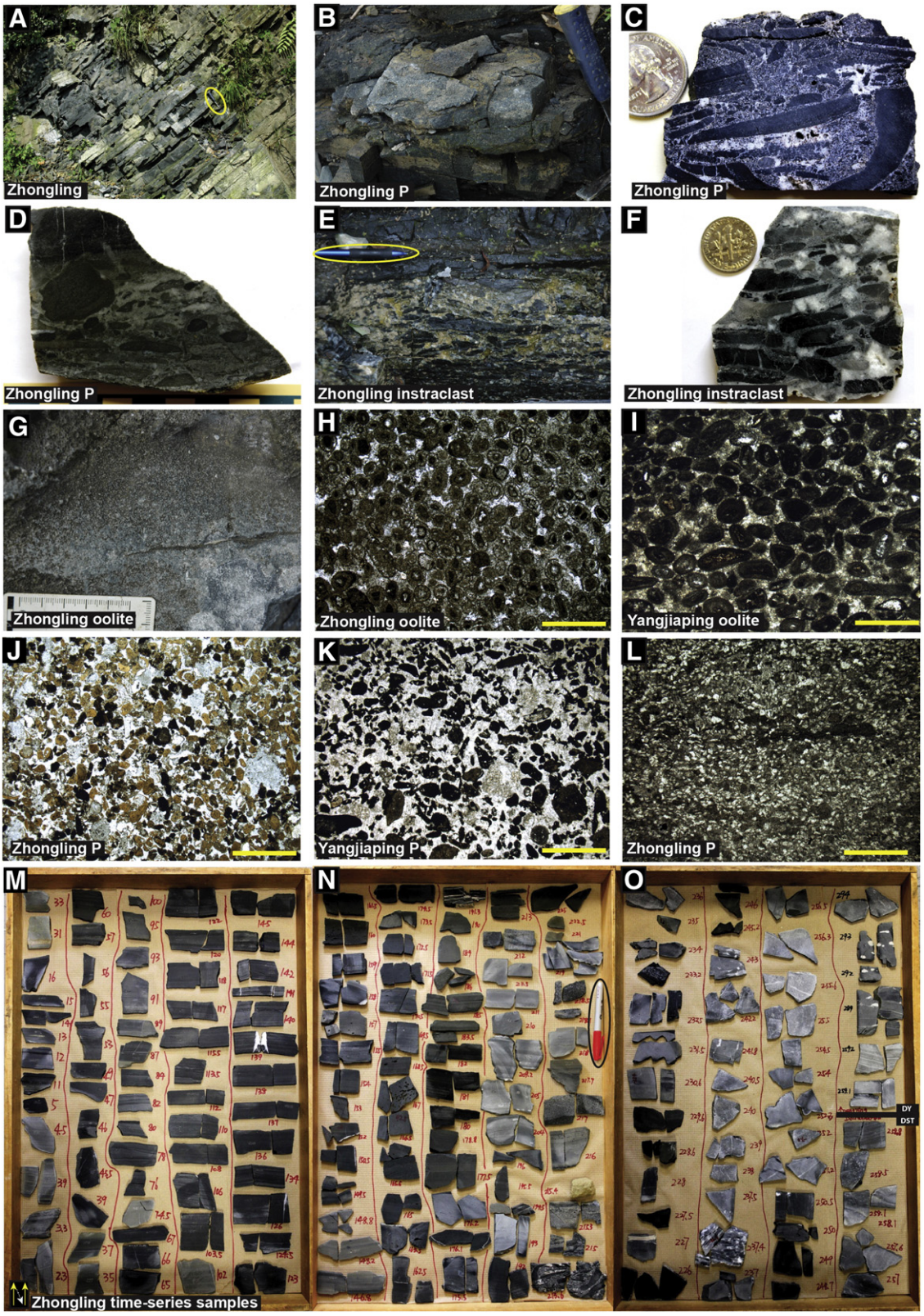

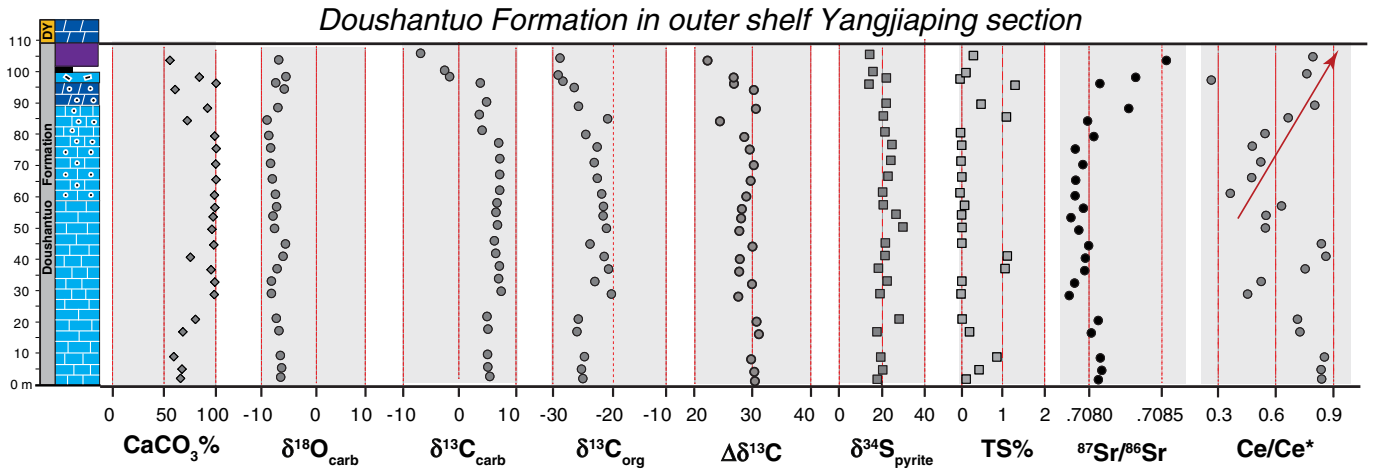

Fig. 3. Integrated time-series elemental and isotopic data from the middle-upper Doushantuo Formation at the outer shelf Yangjiaping section.

secondary veins, and areas with visible silt and clay. Geochemical tests of diagenesis included the comparison of carbonate carbon and oxygen isotope abundances relative to the meteoric alteration trend defined by Knauth and Kennedy (2009). Our micro-samples fell away from this trend, and furthermore were rich in Sr (ranging from 286 to >1600 ppm in all specimens) and had very low Mn/Sr, Fe/Sr, and Rb/Sr ratios (Fig. 4) as expected for well-preserved phases. It is nonetheless clear that the development of the phosphorite horizon(s) (likely to be early diagenetic in origin) in the uppermost Doushantuo Formation at Yangjiaping and Zhongling are associated with the isotope shifts, and thus complicates our interpretation of secular variations in seawater chemistry across the basin. The samples from the upper interval are petrographically fine-grained and organic-rich, in comparison with bedded limestone lower in the succession these are geochemically well preserved.

5.2. Chemostratigraphic correlations of the platform sections

If the lithological and isotope shifts at the top of the Yangjiaping section are widespread and reflect changes in the redox and isotope architecture of the Doushantuo basin, they should also be present at the nearby Zhongling section (Figs. 5–9; Zhu et al., 2007; Li et al., 2010) and at the more proximal sections at Jiulongwan (McFadden et al., 2008) and Xiaofenghe (Xiao et al., 2012; Liu et al., 2013; Zhu et al., 2013). The Zhongling section is located 4 km from the Yangjiaping section and both are lithostratigraphically similar. At Zhongling, the Doushantuo Formation begins with 5 m of cap carbonate atop the Nantuo glacial diamictite, followed by interbedded shale and carbonate, ~20 m of black shale, and finally ~140 m of limestone. The uppermost 50 m of the Doushantuo Formation at Zhongling is dominantly composed of micritic, intraclastic, and oolitic dolostone and organic-rich shale with three prominent levels of phosphorite (Fig. 2). The shale and phosphorite horizons are believed by some researchers to be correlative with the uppermost Doushantuo throughout the basin. Pyrite sulfur and carbon isotope trends at the Zhongling section (Li et al., 2010; new data in this study) are remarkably similar to those in the Yangjiaping section (Fig. 6).

The most accessible and well-studied section of the Doushantuo Formation is near Jiulongwan, where the succession consists of mixed carbonate and shale facies deposited in an intra-shelf environment (Figs. 5–9). There the lower half of the succession above the Nantuo diamictite includes the ca. 635 Ma cap dolostone (Member I) and a thick interval of argillaceous dolostone and mudstone (Member II). The upper half of the unit consists of medium-bedded dolostone overlain by interbedded dolostone and limestone (Member III), which is in turn overlain by black shale with large carbonate concretions (Member IV). No thick phosphorite is present in the upper Doushantuo Formation at this locality although there is minor phosphate enrichment in dolostone facies (McFadden et al., 2008). Sedimentary textures include ribbon rock, microbialaminite, grainstone, and intraclastic packstone, suggesting deposition in shallow subtidal marine environments. The Jiulongwan section preserves three negative carbon isotope excursions, including EN1 (down to −5‰) in the cap carbonate, EN2 (ca. −5‰) at the top of Member II and associated with rapid shallowing of facies (Jiang et al., 2007), and EN3 (ca. −10‰), which is remarkably stable and continues for nearly 50 m through the upper half of Member III and large carbonate concretions in Member IV (Fig. 5; Zhou and Xiao, 2007; McFadden et al., 2008). Based on the shape of this $\delta^{13}C$ excursion, we follow McFadden et al. (2008) and use the subdivisions of EN3a, EN3b and EN3c to represent the decreasing, stable, and recovery intervals of the EN3 $\delta^{13}C$ excursion, respectively. This

Fig. 2. Sedimentological observations of the Doushantuo Formatoin at outer shelf Zhongling and Yangjiaping sections. (A) Thin bedded, dark gray limestone of the Doushantuo Formation at Zhongling, about 120 m above the Nantuo diamictite. The geological hammer is circled as a scale. (B) Intraclastic phosphorite interbedded with black shale about 42 m below the Doushantuo/Dengying (DST/DY) boundary at Zhongling. (C) Phosphorite (12ZL-45.4) about 45.4 m below the DST/DY boundary at Zhongling. (D) Intraclastic phospharite (14ZL-1.3) about 1.3 m below the DST/DY boundary at Zhongling. (E) Intraclastic dolostone about 22 m below the DST-DY boundary at Zhongling. The pencil is circled as a scale. (F) Intraclastic dolostone (12ZL-21.6) about 21.6 m below the DST/DY boundary at Zhongling. (G) Oolitic dolostone about 18.5 m below the DST-DY boundary at Zhongling. (H) Petrographic thin section of oolitic dolostone (12ZL-21) with calcite cements under plane polarized light. Sample was collected about 21 m below the DST/DY boundary at Zhongling. (I) Petrographic thin section of oolitic limestone (Yd-21) under plane polarized light. Sample was collected about 26 m below the DST/DY boundary at Yangjiaping. (J) Petrographic thin section of intraclastic phosphorite (12ZL-42) under plane polarized light. Sample was collected about 42 m below the DST/DY boundary at Zhongling. (K) Petrographic thin section of phosphorite (Yd-26) under plane polarized light. Sample was collected from the uppermost Doushantuo Formation at Yangjiaping. (L) Petrographic thin section of phosphorite (12ZL-0.9) under plane polarized light. Sample was collected from the uppermost Doushantuo Formation at Zhongling. (M, N, O) Time-series samples from the Doushantuo and Dengying formations at Zhongling. Numbers mark stratigrahic heights above the Nantuo diamictite. The marker pen is circled as a scale. The lower ~200 m of the Doushantuo Formation mainly consists of dark-colored carbonates or shale, and above ~200 m height, more and more light-colored dolostone with intraclasts and ooids dominated the upper section, indicating shallower, higher-energy environment. Scales in petrographic images (H–L) are 2 mm. Coins in (C) and (F) are 24 mm and 17 mm in diameter respectively.

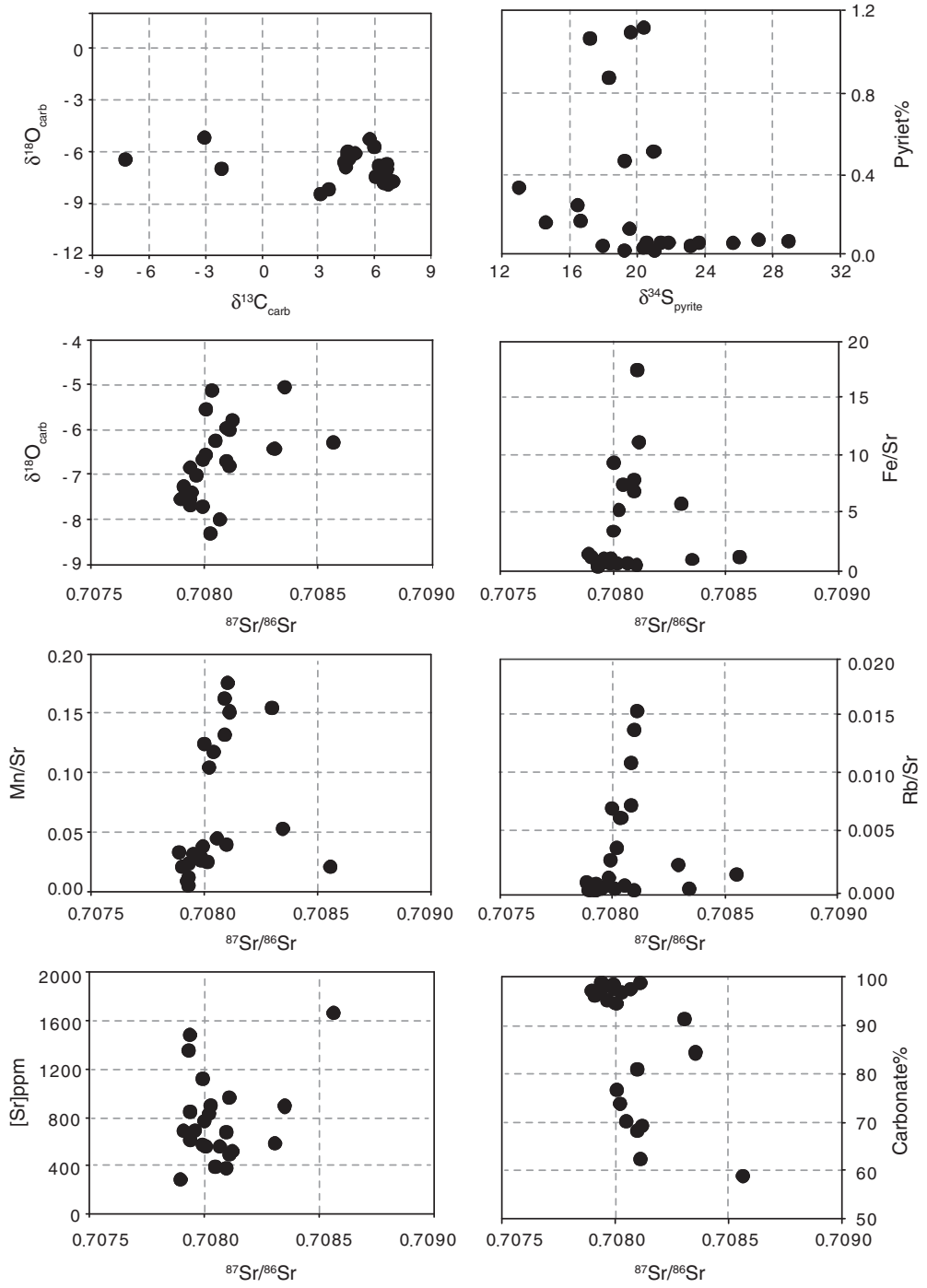

Fig. 4. Cross plots of isotope and elemental data of the middle-upper Doushantuo Formation at Yangjiaping.

geochemical event is widely regarded as correlative with the globally expressed carbon cycle anomaly known as the Shuram Excursion (Fike et al., 2006; Zhu et al., 2007; Grotzinger et al., 2011; Lu et al., 2013; Zhu et al., 2013). Time-series pyrite $\delta^{34}S$ values associated with EN3 at Jiulongwan record a negative trend from 0‰ to as low as −10‰ (Fig. 6), with a similar magnitude decreasing trend in the $\delta^{34}S$ composition of carbonate associated sulfate (McFadden et al., 2008).

The stark contrast in the time-series $\delta^{34}S$ compositions between the uppermost beds at Jiulongwan and Zhongling was used to support the sulfate gradient model (Fig. 1C; Li et al., 2010) for the Doushantuo ocean margin, with the assumption that the Doushantuo Formation in Zhongling section is continuous and can be fully correlated with the Jiulongwan section (see Fig. S7 of Li et al., 2010). However, the Shuram Excursion at Zhongling is poorly expressed, and in our section at Yangjiaping carbonate $\delta^{13}C$ values decline to a low value of −7‰ at the top of the section (Fig. 5), which is likely equivalent to EN3a. It appears possible that both EN3b and EN3c are missing in both of the shoal complex localities, either due to stratigraphic truncation of the upper Doushantuo Formation, or to the diachronous nature of the Doushantuo/Dengying boundary. If the latter is true, the Shuram Excursion should be expressed in the lower Dengying Formation at these localities.

To further evaluate correlations between the inner and outer shelf sections of the Doushantuo Formation, we compared $^{87}Sr/^{86}Sr$ trends constructed from well preserved high-Sr limestone samples (Fig. 7). At the intra-shelf Jiulongwan section, $^{87}Sr/^{86}Sr$ values are consistently

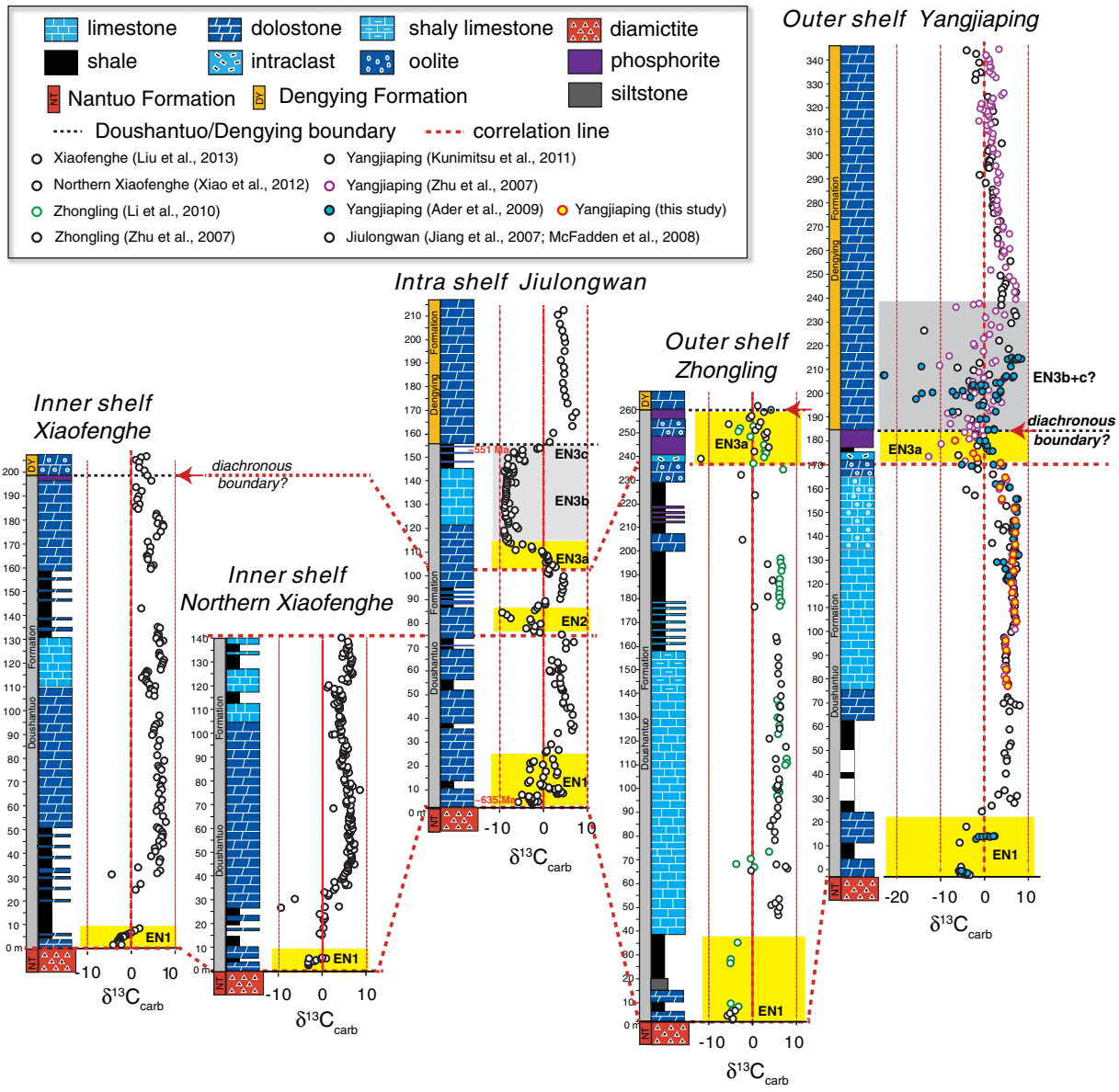

Fig. 5. Carbonate carbon isotope ($\delta^{13}C_{carb}$) chemostratigraphic correlation of the Edaicaran Doushantuo Formation across the platform. Based on carbon, sulfur (Fig. 6), strontium isotope (Fig. 7), and Ce/Ce* (Fig. 8) trends, the shallow inner shelf sections at Xiaofenghe and outer shelf Zhongling and Yangjiaping sections are stratigraphically incomplete (see red dashed correlation lines). The Shuram Excursion (EN3) at Jiulongwan is completely missed in Northern Xiaofenghe and only partially recorded in the Doushantuo Formation at Zhongling and Yangjiaping. The red arrows point to possible diachronous boundary between Doushantuo and Dengying Formation.

low (ca. 0.7080) through most of the section, with a notable rise up to 0.7090 during the Shuram Excursion (Sawaki et al., 2010). Sawaki et al.'s (2010) data are replotted in Fig. 7, with the omission of their whole rock ICP-MS Sr isotope data from impure carbonates with high Mn/Sr (rejection criteria: carbonate wt.% < 60 and Mn/Sr > 1). Although Sawaki et al.'s data were derived from analyses of both dolostones and limestones and our TIMS analyses were exclusively from micro-sampled limestone samples, the stratigraphic patterns of $^{87}Sr/^{86}Sr$ are similar at Jiulongwan, Zhongling, and Yangjiaping (Fig. 7), with the exception of values >0.7085 in EN3b and EN3c at Jiulongwan that are missing in the shoal complex localities. Considering that a stratigraphic rise in $^{87}Sr/^{86}Sr$ from 0.7080 to 0.7090 also occurs across the Shuram Excursion at its type locality in Oman (Burns et al., 1994; Le Guerroué et al., 2006), it is likely that the $^{87}Sr/^{86}Sr$ profile (and the stratigraphy) at Jiulongwan is more complete than those at Zhongling and Yangjiaping.

Two possible interpretations can account for the incomplete Shuram-equivalent EN3 intervals in the outer shelf sections. (1) EN3b and EN3c may have been stratigraphically truncated during a sea level fall, so that these chemostratigraphic features were removed through erosion from the shoal complex facies; this interpretation is consistent with independent sedimentological evidence at these localities, which are dominated by phosphatic intraclasts and oolitic carbonates deposited in shallow high-energy environments (Fig. 2). (2) Alternatively, the lithostratigraphic boundary between the Doushantuo and Dengying formations may be diachronous, so that EN3b and EN3c in the rim sections were instead preserved in dolostone of the lower Dengying Formation. Support for this view comes from strongly negative $\delta^{13}C_{carb}$ data from the lower Dengying Formation at the Yangjiaping section (Figs. 5–7; Zhu et al., 2007; Ader et al., 2009; Ader et al., 2014). This possibility needs to be further tested by other high-resolution chemostratigraphic data (e.g., $^{87}Sr/^{86}Sr$ if limestone facies are preserved) which are currently unavailable.

In earlier publications (Xiao et al., 2012; Zhu et al., 2013), we came to a similar conclusion about the truncation of strata for the Doushantuo

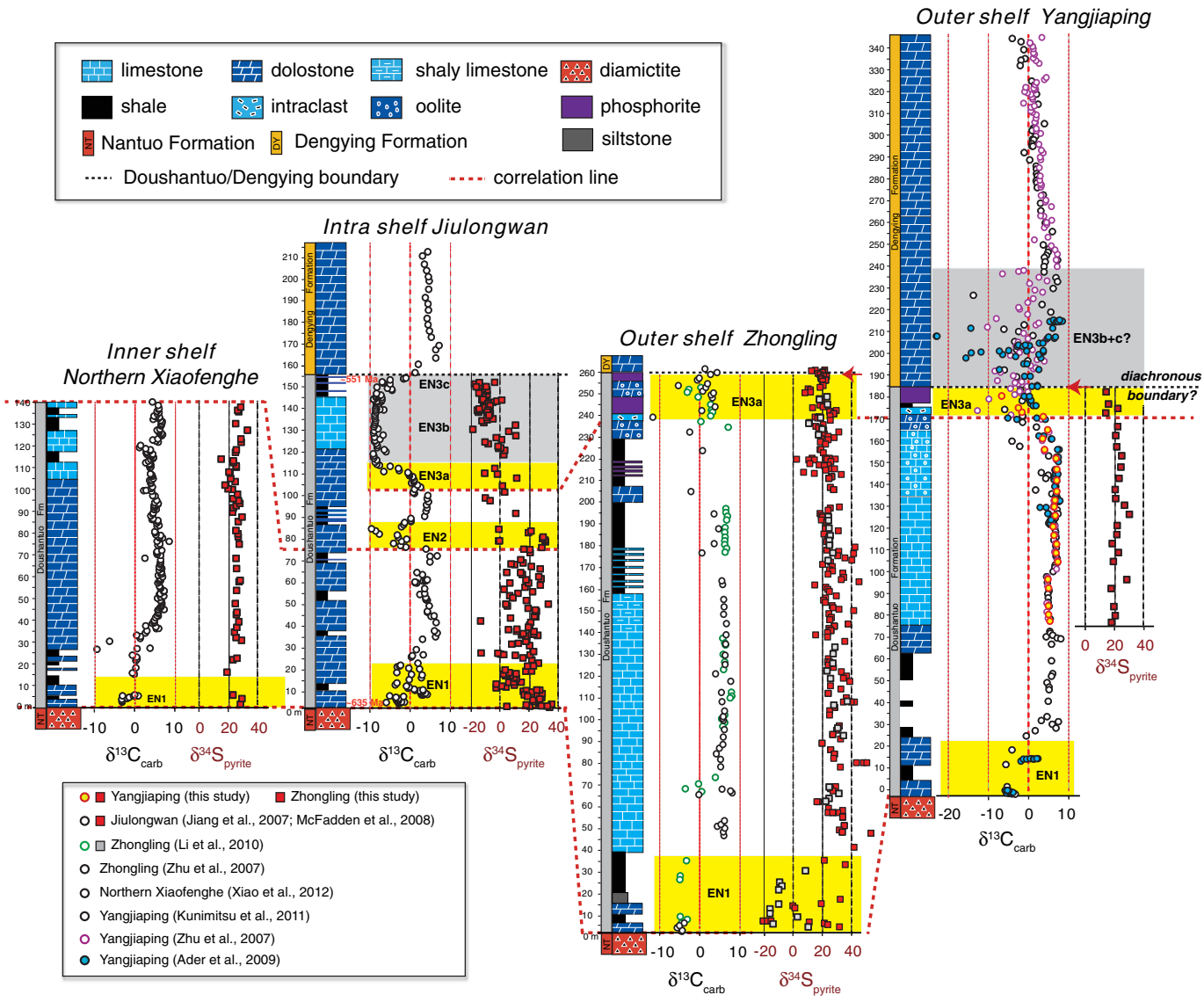

Fig. 6. Pyrite sulfur isotope ($\delta^{34}S_{pyrite}$) chemostratigraphic correlation of the Ediacaran Doushantuo Formation across the platform. $\delta^{34}S_{pyrite}$ of the Shuram Excursion (EN3) at Jiulongwan is characterized by a decreasing trend from slightly positive values to strongly negative values, which is not recorded in either the inner or outer shelf sections. The red arrows point to possible diachronous boundary between Doushantuo and Dengying Formation.

Formation at the Xiaofenghe section, which was deposited in shallower inner shelf facies. The northern Xiaofenghe section (NXF) consists of a basal cap dolostone overlain by a succession of shale, phosphatic packstone or grainstone, and cherty dolostone passing upward into argillaceous limestone (Fig. 5). According the Zhu et al. (2013b), the NXF can be traced to the southern Xiaofenghe section (SXF) where the succession, composed of shale and dolostone, continues upward. Regardless, neither the NXF nor SXF successions reveal carbon, sulfur, or strontium isotopic evidence of the Shuram Excursion (Fig. 5).

In this study, we additionally employed time-series Ce anomaly (Ce/Ce*) as a tool for stratigraphic correlation and to evaluate redox changes through the stratigraphic package (Fig. 8). Although REE concentrations in marine carbonates are notoriously low, and may easily be contaminated by the presence of high-REE clay minerals, we used a significantly diluted leach acid (0.4 M HNO_3) to avoid any admixture of non-carbonate phases. The time-series Ce/Ce* trend reported by Zhou et al. (2012) from the Jiulongwan section reveals a continuous increase from 0.4 to 0.8 through EN3a, followed by a plateau of 0.8 values in EN3b (Fig. 8). We find a similar trend in the top 50 m of the Doushantuo Formation at Yangjiaping, with a steady increase in Ce/Ce* from 0.4 to 0.8 in our interpreted EN3a; the stabilized 0.8 plateau through EN3b at Jiulongwan is missing at Yangjiaping due to the inferred stratigraphic incompleteness of the section.

In summary, the integrated chemostratigraphic correlation of the Doushantuo Formation using $\delta^{13}C$–$\delta^{34}S$–$^{87}Sr/^{86}Sr$–Ce/Ce* suggests that the shallow inner shelf section (Xiaofenghe) and the outer shelf sections (Yangjiaping and Zhongling) are incomplete, with the preserved strata equivalent to the lower 1/2 and 3/4, respectively, of the well-studied Jiulongwan section that accumulated in intra-shelf lagoonal facies (Figs. 5–8).

5.3. Redox and isotopic architecture of the Doushantuo ocean margin

In light of the integrated chemostratigraphic correlations that suggest either stratigraphic truncation of the uppermost Doushantuo Formation in the inner and outer shelf sections, or diachroneity of the Doushantuo/Dengying boundary in the rimmed margin environments, the euxinic wedge model should be reconsidered given that it is based on a stratigraphic miscorrelation. The Shuram Excursion with associated ^{34}S depletion in pyrite and CAS (McFadden et al., 2008) and elevated

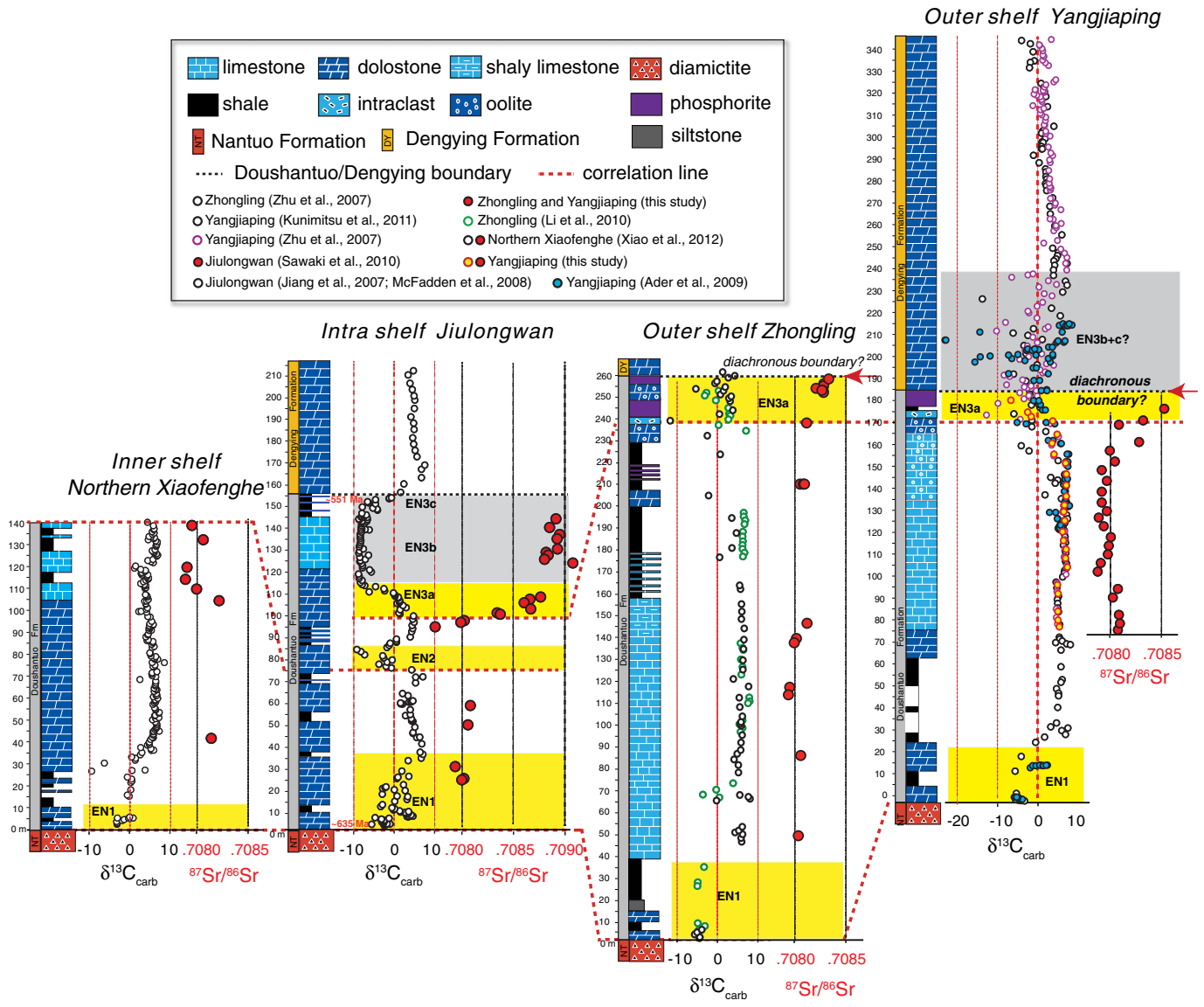

Fig. 7. Strontium isotope ($^{87}Sr/^{86}Sr$) chemostratigraphic correlation of the Ediacaran Doushantuo Formation across the platform. $^{87}Sr/^{86}Sr$ trend in upper Doushantuo Formation at Jiulongwan shows a monotonic increase from 0.7080 to 0.7090, which is consistent with the $^{87}Sr/^{86}Sr$ trend of Shuram Excursion interval from Oman, Siberia and South Australia (see Fig. 10). High-resolution $^{87}Sr/^{86}Sr$ data of upper Doushantuo Formation in outer shelf Zhongling and Yangjiaping sections suggest that the upper Shuram Excursion or EN3b + c (characterized by $^{87}Sr/^{86}Sr$ values of 0.7085–0.7090) is missing from the Doushantuo Formation at outer shelf sections. The red arrows point to possible diachronous boundary between Doushantuo and Dengying Formation.

Fe_{py}/Fe_{HR} (Li et al., 2010) is well preserved in the intra shelf basin succession at Jiulongwan. These indicators suggest that the enxinic water mass on the platform was largely restricted to the intra shelf lagoon, and may not be indicative of a euxinic wedge across the basin margin. While it remains possible that there was a strong surface-to-deep sulfate gradient across the Doushantuo platform, the data currently available do not require a euxinic wedge above a ramp geometry shelf.

Our time-series REE analyses provide additional constraints on changing redox conditions in the Doushantuo basin. Cerium exists in two redox states in marine environments: Ce(III) and Ce(IV). Trivalent Ce can be oxidized into tetravalent Ce in oxic environments, and then be scavenged by Mn-oxides and hydroxides and removed from the ocean. Thus, in oxygenated seawaters, tetravalent Ce is preferentially removed from the system, leaving the seawaters with a Ce negative anomaly in REE patterns. In contrast, Ce is more soluble in reduced environments, resulting in relatively high Ce/Ce* values. Therefore, Ce anomalies (Ce/Ce*) can be used to trace oxygenation changes in seawater (Ling et al., 2013). Our data show that, while the Ce/Ce* ratios oscillate in the middle-upper Doushantuo Formation at Zhongling there is a significant shift in Ce/Ce* from 0.4 to 0.8 starting at about 60 m below the top of the formation (Fig. 8). Notwithstanding a single anomalous outlier, the overall Ce/Ce* trend preserved in the upper Doushantuo Formation at Yangjiaping is coupled with the declining trend in $\delta^{13}C_{carb}$ related to EN3a. This is consistent with similar patterns observed at Jiulongwan (Fig. 8) that support the view that negative $\delta^{13}C$ anomalies are related to widespread anoxia in a stratified depositional basin with enhanced production of ^{13}C-depleted authigenic carbonates (Higgins et al., 2009; Schrag et al., 2013).

Stratification of the Doushantuo seaway, including a pronounced surface-to-deep $\delta^{13}C$ gradient has previously been suggested from the carbonate record (Jiang et al., 2007; Ader et al., 2009). The stratified redox model suggests that the surface ocean preserves the primary signal of carbonate carbon isotope variations; on the other hand, deep ocean sediments may have included a mixture of carbonate transported by pelagic rain or turbidites from shallow environments, as well as ^{13}C-depleted authigenic carbonates (cf. Schrag et al., 2013) that formed in

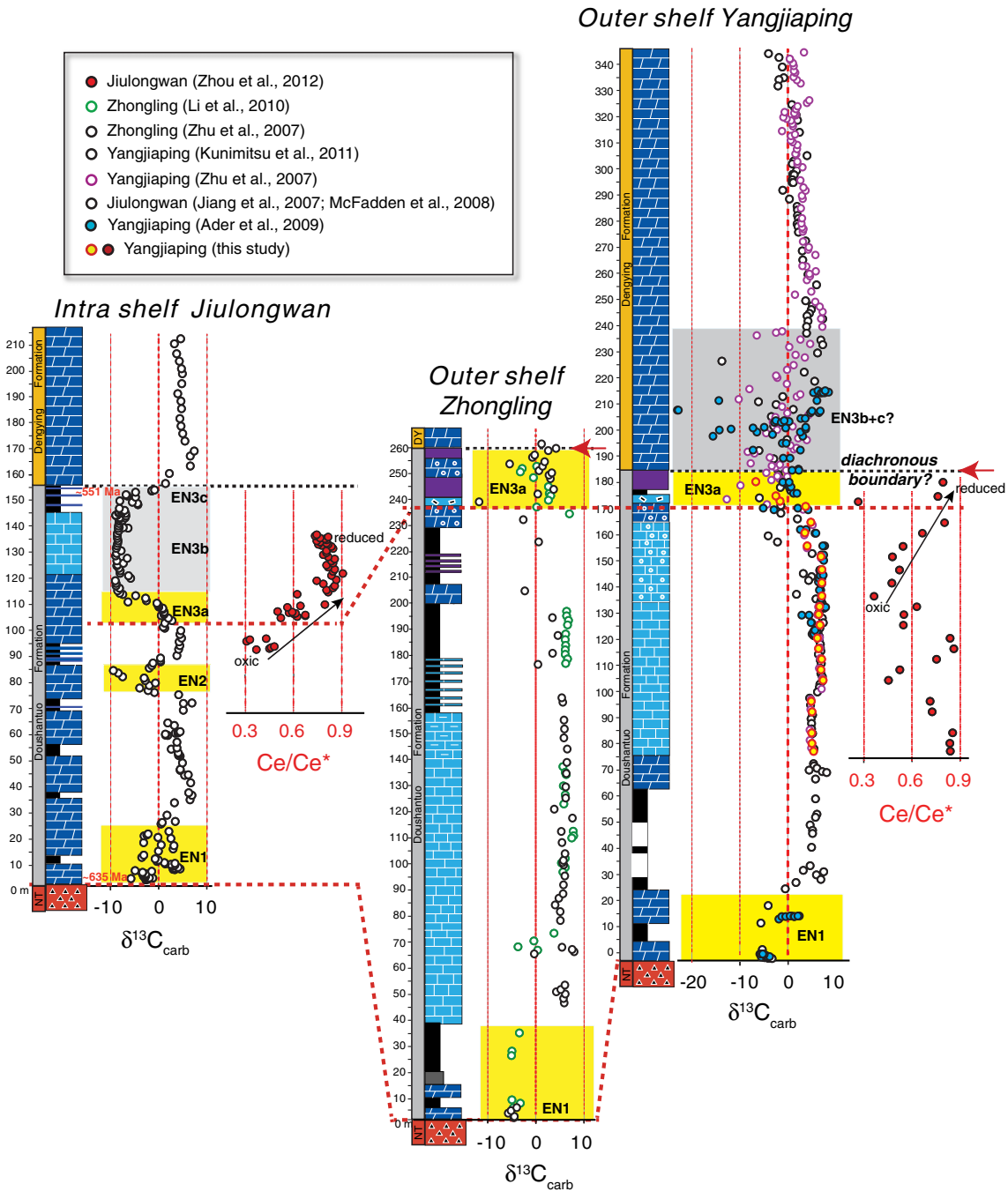

Fig. 8. Ce anomaly (Ce/Ce*) chemostratigraphic correlation of the Ediacaran Doushantuo Formation between the intra-shelf Jiulongwan section and outer shelf Yangjiaping section. Data in both sections are calculated using the formula $Ce/Ce^* = Ce_{PAAS} / ([Pr]^2_{PAAS} / [Nd]_{PAAS})$ (Ling et al., 2013). At Jiulongwan, Ce/Ce* data progressively increase from 0.3 to 0.8 across EN3a (Zhou et al., 2012), and remain at a plateau of 0.8 during EN3b. The upper Doushantuo Formation at Yangjiaping also preserves a similar increasing trend of Ce/Ce* from around 0.4 to around 0.8 (60–105 m stratigraphic height), but the 0.8 plateau recorded in Jiulongwan is missing at Yangjiaping.

association with microbially-mediated iron or sulfate reduction in anoxic environment.

Based on our detailed analysis of platform sections, we additionally note that there may have been a gradient of seawater organic carbon isotope compositions across the basin, with ^{13}C enrichment of up to 5‰ in the outer shelf section at Yangjiaping and Zhongling relative to the inner shelf sections at Xiaofenghe and Jiulongwan (Fig. 9). This organic carbon gradient may persist into the late Ediacaran Period and is recorded in multiple sections of the Dengying Formation (Wang et al., 2014). It is possible that these differences reflect a depth-dependent DOC pool with variable biological sources of organic matter, or alternatively that there was a buildup of ^{13}C-poor respired CO_2 in the intra-shelf lagoon that was subsequently incorporated by photoautotrophs and buried as organic carbon.

5.4. Implications for the Shuram Excursion

Members III and IV of the Ediacaran Doushantuo Formation at Jiulongwan provide the clearest window into the Shuram Excursion in South China. However, the duration of this event, which is preserved through about 50 m of strata, is poorly constrained. The event was clearly over by 551 ± 0.7 Ma (Condon et al., 2005) based on a U–Pb zircon age for a volcanic ash at the stratigraphic contact between the Doushantuo and Dengying formations, but there is no radiometric

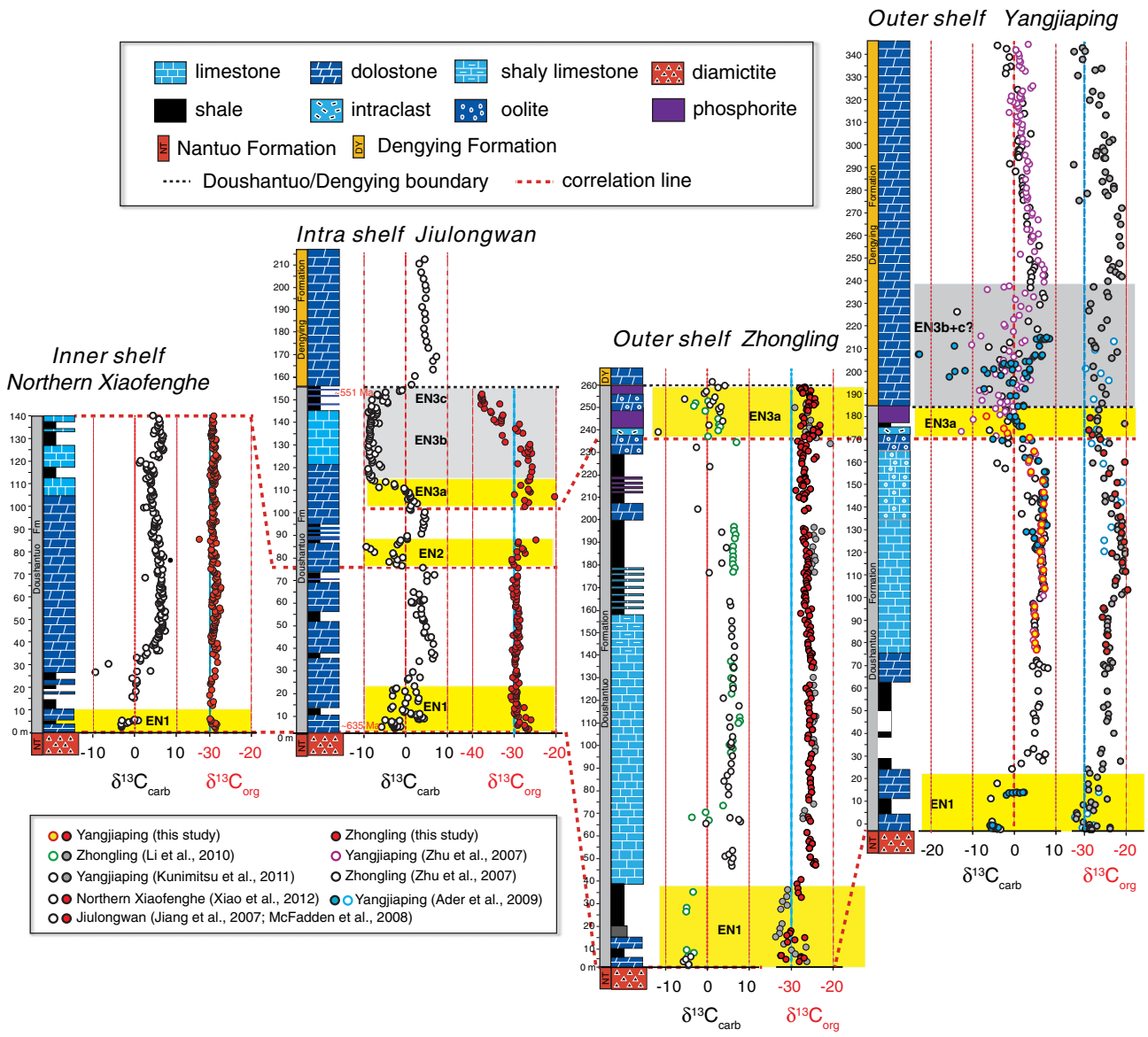

Fig. 9. Paired carbonate carbon ($\delta^{13}C_{carb}$) and organic carbon ($\delta^{13}C_{org}$) isotopic trends of the Edaicaran Doushantuo Formation across the platform. $\delta^{13}C_{org}$ in the outer shelf (Zhongling and Yangjiaping, ca. −25‰) is ~5‰ greater than the inner shelf (Northern Xiaofenghe, ca. −30‰) and intra-shelf (Jiulongwan, ca. −30‰) sections, indicating an organic carbon isotope gradient across the platform.

constraint for the onset of the excursion in the middle of Doushantuo Member III. An imprecise Re–Os age of 595 ± 22 Ma (Zhu et al., 2013) was recently determined from an organic-rich shale horizon at the base of Member IV, but this age provides only a minimum constraint of ca. 35 Myr for the duration of the event. With the caveat that stratigraphic thickness does not necessarily equate to time, Le Guerroué et al. (2006) applied a thermal subsidence model to the >400 m of strata encompassing the Shuram Excursion in Oman to suggest the event lasted at least 50 Myr. Here, we consider that the rise in $^{87}Sr/^{86}Sr$ during the Shuram event may provide an alternative estimate on the duration of the profound carbon cycle anomaly.

At Yangjiaping and Zhongling, our high-[Sr] limestone samples from the upper Doushantuo reveal a rise in $^{87}Sr/^{86}Sr$ compositions from a plateau of values near 0.7080 lower in the succession to 0.7085. Measurements of $^{87}Sr/^{86}Sr$ compositions in the upper Doushantuo at Jiulongwan, which captures the entirety of the Shuram Excursion, suggest that values may rise as high as 0.7090 (Sawaki et al., 2010) during the event. Confidence that the upper Doushantuo $^{87}Sr/^{86}Sr$ shift at Yangjiaping and Zhongling is primary and related to changes in seawater composition comes from our petrographic and geochemical observations, as well as regional and global comparisons (Fig. 10), in particular with the oolitic and stromatolitic limestones with remarkably high Sr abundances from the Patom Uplift of southern Siberia (Melezhik et al., 2009). There $^{87}Sr/^{86}Sr$ values through the lower half of the Shuram Excursion rise monotonically from 0.7080 to 0.7085. A similar trend is recorded in Oman, where $^{87}Sr/^{86}Sr$ compositions rise steadily from 0.7080 to 0.7090 through the carbon cycle anomaly (Burns et al., 1994; Le Guerroué et al., 2006). As an analogue, a similar rise in $^{87}Sr/^{86}Sr$ (0.0005) is noted in the Cenozoic from the Oligocene to the middle Miocene associated with the rise of the Himalayas and the Tibetan plateau (McArthur et al., 2012). Assuming the Cenozoic event monitors the *maximal* possible rate of Sr isotope change, the duration of the Shuram Excursion would minimally be 15 Myr if values rose only to 0.7085, but would extend to 30 Myr if they climbed to 0.7090.

The driving force behind the Cenozoic and Ediacaran rise in $^{87}Sr/^{86}Sr$ recorded in seawater proxies is considered by many to be the result of enhanced delivery of radiogenic ^{87}Sr from the weathering of continental crust (DePaolo and Ingram, 1985; Derry et al., 1992; Richter et al., 1992;

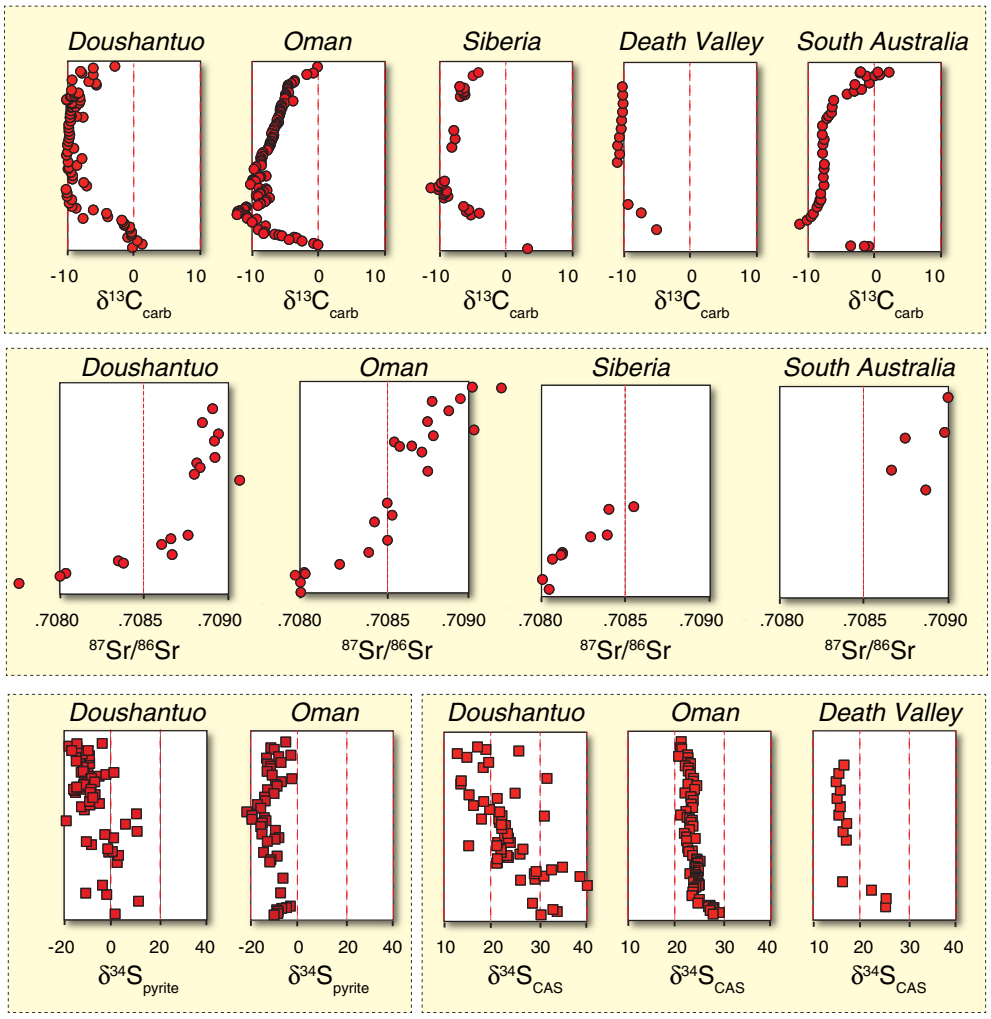

Fig. 10. Compiled carbon, sulfur, and strontium isotope trends in association with the Shuram Excursion recorded in the upper Doushantuo Formation in South China (Jiang et al., 2007; McFadden et al., 2008; Sawaki et al., 2010) and presumably equivalent strata in Oman (Burns et al., 1994; Fike et al., 2006; Le Guerroué et al., 2006), Siberia (Pokrovskii et al., 2006a, 2006b; Melezhik et al., 2009; Pokrovsky and Bujakaite, 2015), Death Valley (Kaufman et al., 2007), and South Australia (Wonoka Formation; Calver, 2000). The stratigraphic thickness of the Shuram Excursion is different at different sections, and thus the chemostratigraphic profiles are not shown to scale.

Kaufman et al., 1993; Paytan et al., 1993). Alternatively, the Sr isotope shift might also reflect a decrease in mantle Sr inputs or an increase in the $^{87}Sr/^{86}Sr$ of exposed rocks undergoing weathering (Shields, 2007). Based on: 1) the range of Sr isotope compositions of riverine sources today (Palmer and Edmond, 1992), 2) measurements of the isotopic composition of detrital Sr in shales (Goldstein, 1988), and 3) the unlikely scenario that seafloor spreading rates decreased during an interval of rapid continental reorganization, it is unlikely that either hydrothermal inputs of Sr decreased or that the radiogenic composition of exposed continental rocks increased (Shields, 2007) in the middle Ediacaran Period. Accepting this argument, the most likely explanation for the Shuram rise in $^{87}Sr/^{86}Sr$ remains an overall increase in continental weathering rates.

Support for the weathering hypothesis comes from coupled measurements of carbonate carbon and sulfur (both pyrite and CAS) isotope compositions in samples from Ediacaran successions in Oman (Fike et al., 2006), the western USA (Kaufman et al., 2007) and South China (McFadden et al., 2008), each of which reveals pronounced $\delta^{34}S$ negative isotope shifts (Fig. 10) suggesting enhanced delivery of sulfate into the ocean. The effects of weathering would have been enhanced if the Shuram Excursion was coincided with a stepwise rise in the redox state of the Ediacaran ocean and atmosphere (aka Neoproterozoic Oxidation Event or NOE) (Fike et al., 2006; Canfield et al., 2007; Shields-Zhou and Och, 2011; Och and Shields-Zhou, 2012).

6. Conclusions

Our integrated basin-wide chemostratigraphic correlations of the Ediacaran Doushantuo Formation based on time-series carbon, sulfur, strontium isotope and Ce anomaly measurements suggest that the Doushantuo Formation in shallow marine environments at both proximal and distal rimmed settings are stratigraphically incomplete to variable degrees compared with the well-studied intra shelf Jiulongwan section. Such incompleteness can be explained by possible stratigraphic truncation in shallow environments. Alternatively, our time-series results may indicate that the lithostratigraphic boundary between the Doushantuo and Dengying formations may be diachronous across the platform. This view must be considered in geochemical models of the redox architecture of this (and other) Ediacaran basin(s), as well as our understanding of the distribution of early multicellular eukaryotes preserved in these ancient sedimentary archives.

Acknowledgments

We thank Richard Walker, Igor Puchtel, Jingao Liu and Katherine Bermingham for the guidance of Sr isotope measurements in the UMD Isotope Geochemistry Laboratory. We also thank Yongbo Peng, Mike Evans, Rebecca Plummer, and Brittney Gaeta for their assistance in the UMD Paleoclimate CoLaboratory. This research is supported by funding

from the NASA Exobiology (NNX12AR91G), the National Basic Research Program of China (2013CB835000), the NSF Sedimentary Geology and Paleontology program (EAR0844270), the Explorers Club Exploration Fund Grant, the International Association of Sedimentologist (IAS) Graduate Student Research Grant, and the Society of Economic Geologists (SEG) Student Research Grant.

Appendix A. Supplementary data

Supplementary data to this article can be found online at http://dx.doi.org/10.1016/j.chemgeo.2015.04.009.

References

Ader, M., et al., 2009. A multilayered water column in the Ediacaran Yangtze platform? Insights from carbonate and organic matter paired δ13C. Earth Planet. Sci. Lett. 288 (1–2), 213–227.
Ader, M., et al., 2014. Ocean redox structure across the Late Neoproterozoic oxygenation event: a nitrogen isotope perspective. Earth Planet. Sci. Lett. 396, 1–13.
Bjerrum, C.J., Canfield, D.E., 2011. Towards a quantitative understanding of the late Neoproterozoic carbon cycle. Proc. Natl. Acad. Sci. U. S. A. 108 (14), 5542–5547.
Burns, S., Matter, A., 1993. Carbon isotopic record of the latest Proterozoic from Oman. Eclogae Geol. Helv. 86 (2), 595–607.
Burns, S.J., Haudenschild, U., Matter, A., 1994. The strontium isotopic composition of carbonates from the late Precambrian (~560–540 Ma) Huqf Group of Oman. Chem. Geol. 111 (1–4), 269–282.
Calver, C.R., 2000. Isotope stratigraphy of the Ediacarian (Neoproterozoic III) of the Adelaide Rift Complex, Australia, and the overprint of water column stratification. Precambrian Res. 100 (1–3), 121–150.
Canfield, D.E., Poulton, S.W., Narbonne, G.M., 2007. Late-Neoproterozoic deep-ocean oxygenation and the rise of animal life. Science 315, 92–95.
Chen, Z., et al., 2013. Trace fossil evidence for Ediacaran bilaterian animals with complex behaviors. Precambrian Res. 224, 690–701.
Chen, Z., et al., 2014. New Ediacara fossils preserved in marine limestone and their ecological implications. Sci. Rep. 4.
Condon, D., et al., 2005. U–Pb ages from the neoproterozoic Doushantuo Formation, China. Science 308 (5718), 95–98.
Coplen, T.B., et al., 2006. New guidelines for δ13C measurements. Anal. Chem. 78 (7), 2439–2441.
DePaolo, D.J., Ingram, B.L., 1985. High-resolution stratigraphy with strontium isotopes. Science 227 (4689), 938–941.
Derry, L.A., 2010. A burial diagenesis origin for the Ediacaran Shuram–Wonoka carbon isotope anomaly. Earth Planet. Sci. Lett. 294 (1–2), 152–162.
Derry, L.A., Kaufman, A.J., Jacobsen, S.B., 1992. Sedimentary cycling and environmental change in the Late Proterozoic: evidence from stable and radiogenic isotopes. Geochim. Cosmochim. Acta 56 (3), 1317–1329.
Deutsch, C., Brix, H., Ito, T., Frenzel, H., Thompson, L., 2011. Climate-forced variability of ocean hypoxia. Science 333 (6040), 336–339.
Fike, D.A., Grotzinger, J.P., Pratt, L.M., Summons, R.E., 2006. Oxidation of the Ediacaran Ocean. Nature 444, 744–747.
Goldstein, S.L., 1988. Decoupled evolution of Nd and Sr isotopes in the continental crust and the mantle. Nature 336, 733–738.
Grotzinger, J.P., Fike, D.A., Fischer, W.W., 2011. Enigmatic origin of the largest-known carbon isotope excursion in Earth's history. Nat. Geosci. 4 (5), 285–292.
Higgins, J., Fischer, W., Schrag, D., 2009. Oxygenation of the ocean and sediments: consequences for the seafloor carbonate factory. Earth Planet. Sci. Lett. 284 (1), 25–33.
Jiang, G., Kaufman, A.J., Christie-Blick, N., Zhang, S., Wu, H., 2007. Carbon isotope variability across the Ediacaran Yangtze platform in South China: implications for a large surface-to-deep ocean δ13C gradient. Earth Planet. Sci. Lett. 261 (1), 303–320.
Jiang, G., Shi, X., Zhang, S., Wang, Y., Xiao, S., 2011. Stratigraphy and paleogeography of the Ediacaran Doushantuo Formation (ca. 635–551 Ma) in South China. Gondwana Res. 19 (4), 831–849.
Kaufman, A.J., Jacobsen, S.B., Knoll, A.H., 1993. The Vendian record of Sr and C isotopic variations in seawater: implications for tectonics and paleoclimate. Earth Planet. Sci. Lett. 120 (3), 409–430.
Kaufman, A.J., Corsetti, F.A., Varni, M.A., 2007. The effect of rising atmospheric oxygen on carbon and sulfur isotope anomalies in the Neoproterozoic Johnnie Formation, Death Valley, USA. Chem. Geol. 237, 47–63.
Knauth, L.P., Kennedy, M.J., 2009. The late Precambrian greening of the Earth. Nature 460, 728–732.
Kunimitsu, Y., Setsuda, Y., Furuyama, S., Wang, W., Kano, A., 2011. Ediacaran chemostratigraphy and paleoceanography at a shallow marine setting in northwestern Hunan Province, South China. Precambrian Res. 191 (3–4), 194–208.
Laflamme, M., Xiao, S., Kowalewski, M., 2009. Osmotrophy in modular Ediacara organisms. Proc. Natl. Acad. Sci. 106 (34), 14438–14443.
Le Guerroué, E., Allen, P.A., Cozzi, A., Etienne, J.L., Fanning, M., 2006. 50 Myr recovery from the largest negative δ13C excursion in the Ediacaran ocean. Terra Nova 18 (2), 147–153.
Li, C., et al., 2010. A stratified redox model for the Ediacaran ocean. Science 328 (5974), 80–83.
Ling, H.-F., et al., 2013. Cerium anomaly variations in Ediacaran—earliest Cambrian carbonates from the Yangtze Gorges area, South China: implications for oxygenation of coeval shallow seawater. Precambrian Res. 225, 110–127.
Liu, P., Yin, C., Chen, S., Tang, F., Gao, L., 2013. The biostratigraphic succession of acanthomorphic acritarchs of the Ediacaran Doushantuo Formation in the Yangtze Gorges area, South China and its biostratigraphic correlation with Australia. Precambrian Res. 225, 29–43.
Liu, P., et al., 2014. Ediacaran acanthomorphic acritarchs and other microfossils from chert nodules of the upper Doushantuo Formation in the Yangtze Gorges area, South China. J. Paleontol. 88 (sp72), 1–139.
Lu, M., et al., 2013. The DOUNCE event at the top of the Ediacaran Doushantuo Formation, South China: Broad stratigraphic occurrence and non-diagenetic origin. Precambrian Res. 225, 86–109.
Macdonald, F.A., et al., 2013. The stratigraphic relationship between the Shuram carbon isotope excursion, the oxygenation of Neoproterozoic oceans, and the first appearance of the Ediacara biota and bilaterian trace fossils in northwestern Canada. Chem. Geol. 362, 250–272.
McArthur, J., Howarth, R., Shields, G., 2012. Strontium isotope stratigraphy. A geologic time scale: 127–144.
McFadden, K.A., et al., 2008. Pulsed oxidation and biological evolution in the Ediacaran Doushantuo Formation. Proc. Natl. Acad. Sci. 105 (9), 3197–3202.
Melezhik, V.A., Pokrovsky, B.G., Fallick, A.E., Kuznetsov, A.B., Bujakaite, M.I., 2009. Constraints on 87Sr/86Sr of Late Ediacaran seawater: insight from Siberian high-Sr limestones. J. Geol. Soc. 166 (1), 183–191.
Meyer, M., et al., 2014. Interactions between Ediacaran animals and microbial mats: insights from Lamonte trevallis, a new trace fossil from the Dengying Formation of South China. Palaeogeogr. Palaeoclimatol. Palaeoecol. 396, 62–74.
Mills, D.B., et al., 2014. Oxygen requirements of the earliest animals. Proc. Natl. Acad. Sci. 111 (11), 4168–4172.
Mora, C., et al., 2013. Biotic and human vulnerability to projected changes in ocean biogeochemistry over the 21st century. PLoS Biol. 11 (10), e1001682.
Muscente, A.D., Hawkins, A.D., Xiao, S., 2015. Fossil preservation through phosphatization and silicification in the Ediacaran Doushantuo Formation (South China): a comparative synthesis. Palaeogeogr. Palaeoclimatol. Palaeoecol. (0).
Och, L.M., Shields-Zhou, G.A., 2012. The Neoproterozoic oxygenation event: environmental perturbations and biogeochemical cycling. Earth Sci. Rev. 110 (1–4), 26–57.
Palmer, M., Edmond, J., 1992. Controls over the strontium isotope composition of river water. Geochim. Cosmochim. Acta 56 (5), 2099–2111.
Paytan, A., Kastner, M., Martin, E., Macdougall, J., Herbert, T., 1993. Marine barite as a monitor of seawater strontium isotope composition. Nature 366 (6454), 445–449.
Pokrovskii, B., Melezhik, V., Bujakaite, M., 2006a. Carbon, oxygen, strontium, and sulfur isotopic compositions in late Precambrian rocks of the Patom Complex, central Siberia: communication 1. Results, isotope stratigraphy, and dating problems. Lithol. Miner. Resour. 41 (5), 450–474.
Pokrovskii, B.G., Melezhik, V.A., Bujakaite, M.I., 2006b. Carbon, oxygen, strontium, and sulfur isotopic compositions in late Precambrian rocks of the Patom Complex, central Siberia: communication 2. Nature of carbonates with ultralow and ultrahigh δ13C values. Lithol. Miner. Resour. 41 (6), 576–587.
Pokrovsky, B.G., Bujakaite, M.I., 2015. Geochemistry of C, O, and Sr isotopes in the Neoproterozoic carbonates from the southwestern Patom paleobasin, southern Middle Siberia. Lithol. Miner. Resour. 50 (2), 144–169.
Richter, F.M., Rowley, D.B., DePaolo, D.J., 1992. Sr isotope evolution of seawater: the role of tectonics. Earth Planet. Sci. Lett. 109 (1), 11–23.
Rothman, D.H., Hayes, J.M., Summons, R.E., 2003. Dynamics of the Neoproterozoic carbon cycle. Proc. Natl. Acad. Sci. 100 (14), 8124–8129.
Sahoo, S.K., et al., 2012. Ocean oxygenation in the wake of the Marinoan glaciation. Nature 489 (7417), 546–549.
Sawaki, Y., et al., 2010. The Ediacaran radiogenic Sr isotope excursion in the Doushantuo Formation in the Three Gorges area, South China. Precambrian Res. 176 (1–4), 46–64.
Schrag, D.P., Higgins, J.A., Macdonald, F.A., Johnston, D.T., 2013. Authigenic carbonate and the history of the global carbon cycle. Science 339 (6119), 540–543.
Shields, G., 2007. A normalised seawater strontium isotope curve: possible implications for Neoproterozoic–Cambrian weathering rates and the further oxygenation of the Earth. eEarth 2 (2), 35–42.
Shields-Zhou, G., Och, L., 2011. The case for a Neoproterozoic oxygenation event: geochemical evidence and biological consequences. GSA Today 21 (3), 4–11.
Spötl, C., 2011. Long-term performance of the Gasbench isotope ratio mass spectrometry system for the stable isotope analysis of carbonate microsamples. Rapid Commun. Mass Spectrom. 25 (11), 1683–1685.
Tahata, M., et al., 2013. Carbon and oxygen isotope chemostratigraphies of the Yangtze platform, South China: decoding temperature and environmental changes through the Ediacaran. Gondwana Res. 23 (1), 333–353.
Wang, L., Shi, X., Jiang, G., 2012a. Pyrite morphology and redox fluctuations recorded in the Ediacaran Doushantuo Formation. Palaeogeogr. Palaeoclimatol. Palaeoecol. 333–334, 218–227.
Wang, W., Zhou, C., Yuan, X., Chen, Z., Xiao, S., 2012b. A pronounced negative δ13C excursion in an Ediacaran succession of western Yangtze Platform: a possible equivalent to the Shuram event and its implication for chemostratigraphic correlation in South China. Gondwana Res. 22 (3–4), 1091–1101.
Wang, X., Shi, X., Jiang, G., Tang, D., 2014. Organic carbon isotope gradient and ocean stratification across the late Ediacaran–Early Cambrian Yangtze Platform. Sci. China Earth Sci. 57 (5), 919–929.
Xiao, S., Laflamme, M., 2009. On the eve of animal radiation: phylogeny, ecology and evolution of the Ediacara biota. Trends Ecol. Evol. 24 (1), 31–40.

Xiao, S., Zhang, Y., Knoll, A.H., 1998. Three-dimensional preservation of algae and animal embryos in a Neoproterozoic phosphorite. Nature 391 (6667), 553–558.
Xiao, S., et al., 2012. Integrated chemostratigraphy of the Doushantuo Formation at the northern Xiaofenghe section (Yangtze Gorges, South China) and its implication for Ediacaran stratigraphic correlation and ocean redox models. Precambrian Res. 192–195, 125–141.
Xiao, S., Zhou, C., Liu, P., Wang, D., Yuan, X., 2014. Phosphatized acanthomorphic acritarchs and related microfossils from the Ediacaran Doushantuo Formation at Weng'an (South China) and their implications for biostratigraphic correlation. J. Paleontol. 88 (1), 1–67.
Yin, Z., et al., 2015. Sponge grade body fossil with cellular resolution dating 60 Myr before the Cambrian. Proc. Natl. Acad. Sci. 112 (12), E1453–E1460 (201414577).
Zhou, C., Xiao, S., 2007. Ediacaran δ13C chemostratigraphy of South China. Chem. Geol. 237 (1–2), 89–108.
Zhou, C., Jiang, S., Xiao, S., Chen, Z., Yuan, X., 2012. Rare earth elements and carbon isotope geochemistry of the Doushantuo Formation in South China: implication for middle Ediacaran shallow marine redox conditions. Chin. Sci. Bull. 57 (16), 1998–2006.
Zhu, M., Zhang, J., Yang, A., 2007. Integrated Ediacaran (Sinian) chronostratigraphy of South China. Palaeogeogr. Palaeoclimatol. Palaeoecol. 254 (1–2), 7–61.
Zhu, B., et al., 2013a. Re–Os geochronology of black shales from the Neoproterozoic Doushantuo Formation, Yangtze platform, South China. Precambrian Res. 225, 67–76.
Zhu, M., et al., 2013b. Carbon isotope chemostratigraphy and sedimentary facies evolution of the Ediacaran Doushantuo Formation in western Hubei, South China. Precambrian Res. 225, 7–28.